IAC–24–A3,5,4,x91151

Design and architecture of Anubis: a hopper to sample and study Mercury's surface and subsurface

Co-Authors
Aurora Cagnoni (aurora.cagnoni@mail.polimi.it), Gianni Curti (gianni.curti@mail.polimi.it), Nicolò Galletta (nicolo.galletta@mail.polimi.it), Joshua Jeyasselan Jeevanantha Bharathi (joshuajeyaseelan.jeevanantha@mail.polimi.it), Luigi Marchese (luigi.marchese@mail.polimi.it), Andrea Pinelli (andrea.pinelli@mail.polimi.it), Matteo Piunti (matteo.piunti@mail.polimi.it), Matteo Rossi (matteo23.rossi@mail.polimi.it), Matteo Santacesaria (matteo.santacesaria@mail.polimi.it), Andrea Sapuppo (andrea1.sapuppo@mail.polimi.it), Aurora Saracini (aurora.saracini@mail.polimi.it), Luca Sportelli (luca.sportelli@mail.polimi.it), Michèle Roberta Lavagna (michelle.lavagna@polimi.it)

In the quest to unravel the mysteries of our cosmic neighbors, the focus is set on Mercury, the closest planet to the Sun. A new era of exploration and discovery awaits as a mission of unprecedented ambition unfolds, one that promises to change the understanding of this rocky world.
Over the years, several missions have investigated Mercury. Nevertheless, they only relied on orbiters, thus conducting remote studies of its surface. On the other hand, Anubis, the core element of the Mercury In-situ Regolith Analysis, Geophysics and Exosphere (MIRAGE) mission, aims to outline a ground segment capable of exploring three distinct regions of Mercury's surface and subsurface allowing an unprecedented science return. The surface of Mercury showcases distinct features characterized by the presence of craters and larger circular regions, predominantly formed due to the impacts of minor celestial bodies. Mariner 10 and MESSENGER revealed interesting reflectance disparities on the surface caused by differences in composition. There are three different categories that can be broadly classified as follows: ancient, heavily cratered terrain with an intermediate albedo; Low Reflectance Material (LRM); High Reflectance Material (HRM). Caloris Basin has been selected as the primary landing site for the presence of plane regions with LRM and HRM in close proximity and for its strongly magnetized nature.
The science objectives are satisfied by a hopper, an innovative vehicle capable of travelling more than 70 km across the surface of Mercury thanks to its propulsion system. Through its jumps a series of different sites, firstly LRM, secondly HRM and finally a young crater, are sampled and studied, providing the analysis of most of the elements present on the planet.
The most revolutionary aspects of Anubis are the descent, landing and jumping capability, allowing enhanced mobility and needing for an innovative power source for surviving the harsh conditions. These characteristics underscore its superior capabilities when compared to traditional rovers.
A major challenge was the survivability on Mercury's surface, which experiences extremely high temperatures during the day. This was addressed by landing at dusk and conducting operations during night. Analysis on radiation, particles, seismic vibrations, magnetic field and chemical composition are performed. To collect the samples a drill was specifically designed, with a capability of reaching up to 20 cm depth.
This preliminary phase A study was realized during a semester, in the context of the course "Applied Space Mission Analysis and Design".

List of Acronyms

ADCS Attitude Determination and Control Subsystem

BOL Beginning Of Life

CEA Chemical Equilibrium with Applications
COCOMO81 COnstructive COst MOdel 1981

DC Direct Current
DD Dust Detector
DOD Depth-Of-Discharge
DoF Degrees of Freedom
DSN Deep Space Network

EOL End Of Life
EPS Energetic Particle Spectrometer

GNC Guidance, Navigation and Control
GRS Gamma Ray Spectrometer

GTO Geostationary Transfer Orbit
GPHS General Purpose Heat Source

HGA High Gain Antenna
HRM High Reflectance Material
HYD Hydrazine

IMS Ion Mass Spectrometer
IMU Inertial Measurement Unit

LOOS Launch Operations and Orbital Support
LRM Low Reflectance Material
LVA Launch Vehicle Adapter

MA Mission Analysis
MESSENGER MErcury Surface, Space ENvironment, GEochemistry, and Ranging
MIRAGE Mercury In-situ Regolith Analysis, Geophysics and Exosphere
MLI Multi-Layer Insulation
MON Mixed Oxides of Nitrogen

NASA National Aeronautics and Space Administration
NMS Neutral Mass Spectrometer

OBC On-Board Computer

RAM Random Access Memory
RTG Radioisotope Thermoelectric Generator
RIU Remote Interface Unit

S/C Spacecraft
SLS Space Launch System

TCS Thermal Control Subsystem
TM Transfer Module
TMTC Telemetry and Telecommand subsystem
T/W Thrust over Weight ratio

USCM8 Unmanned Spacecraft Cost Model
USDC Ultrasonic/Sonic Driller/Corer

XRD/XRF X-Ray Diffractrometer/Fluorescence

I. Introduction

As the innermost planet in our solar system, Mercury presents significant challenges for space exploration due to its proximity to the Sun and extreme environmental conditions. To date, only two missions—Mariner 10 and MESSENGER—have successfully reached Mercury, with a third, BepiColombo, currently on its way and expected to arrive by the end of 2025. These missions have provided valuable insights into Mercury's surface and environment; however, they were limited to orbital observations, relying primarily on remote sensing techniques.
While these orbital missions have vastly expanded our knowledge, many of Mercury's mysteries remain unsolved, particularly regarding its unique geological features, internal structure, and volatile compounds. To address these gaps, the MIRAGE mission proposes a groundbreaking approach: landing a hopper vehicle on Mercury's surface, which will enable the mission to visit and analyze three distinct sites on the planet's surface spanning over 70 km. This mission will not only allow for direct surface measurements but also enable in-depth analysis of Mercury's composition, geology, magnetic field and trapped volatile deposits. Thus offering unprecedented insights into the planet's formation and evolution. The mission will depart from Earth on January 23, 2035, and reach Mercury on December 5, 2042. Upon arrival, the spacecraft will use liquid chemical propulsion to execute a precise orbital insertion around Mercury. Subsequently, an orbiter will continue to revolve around the planet to conduct long-term observations and act as a relay for telecommunication with Earth, while the descent stage will initiate the deployment of the Hopper. Utilizing a combination of solid and liquid chemical propulsion, the descent stage will carefully guide the hopper to a controlled landing on Mercury's surface.

II. Mission Objectives

The primary goals of this mission include:

- **Investigate the mineralogy and chemistry of Mercury's surface:** to discover uncovered elevated sulfur levels and diminished iron content on Mercury's surface, pointing to a reduced oxygen environment;
- **Characterize Mercury's interior structure:** to deepen the knowledge on density, temperature and composition;
- **Characterize Mercury's magnetic field;**
- **Determine the processes that produces Mercury's exosphere and alter its regolith:** the planet's surface is exposed to a challenging environment, making it imperative to investigate the interactions between particles and the surface, as these play a significant role in generating the exosphere and potentially influencing the planet's landscape;

- **Study of the trapped volatiles:** the night region contains extensive deposits of water ice and other volatile compounds, which are directly exposed on the surface, providing a unique opportunity for sampling;

- **Characterize the surface and subsurface with in-situ analyses:** Mercury exhibits a remarkable diversity in terms of its surface compositions.

The study was conducted on three distinct sites on Mercury, as previously mentioned, to optimize the analysis of the Hermean surface. The selection of these sites is crucial, as it directly influences the choice of mission architecture. Consequently, three scientifically significant and relevant locations were identified.
Mercury's surface is characterized by three primary terrains with varying reflectance: a LRM, a HRM, and an intermediate terrain that comprises the majority of Mercury's cratered surface. Additionally, there are three distinct types of terrains identified by other reflectance values, albeit confined to smaller areas: high-reflectance fresh materials originating from immature young craters and their ejecta, bright deposits within the permanently shadowed craters at the poles, and a reddish, moderately reflective material likely associated with pyroclastic vents.
All three of these terrains are located along the rims of Caloris Basin crater; every location is 35 km apart for a total of 70 km covered on the Hermean surface. Caloris Basin, with a diameter of 1550 km, is one of the largest impact basins in the Solar System. It is filled with HRM lava plains and contains smaller impact craters. The region is also characterized by strong magnetism, with extensive LRM terrains present at its rim [1].

III. Configuration

The whole spacecraft is composed of four stages: the Transfer Module, the Orbital Module, divided into solid and liquid based on the propulsion system carried, the Hopper and the Science Orbiter. As it can be seen in Figure 1, all the stages are stack vertically one on top of the others and they are connected thorough the use of interfaces. In order to give more robustness to the whole configuration, the heaviest stages - Hopper, Transfer Module and Orbital Module - are placed such that their structural cylinders are aligned, allowing for a better distribution of structural forces. In order to avoid increasing the Orbital Module dimensions, it was decided to have a Hopper with deployable and retractable legs to decrease the occupied volume and the adapter and sunshield height.

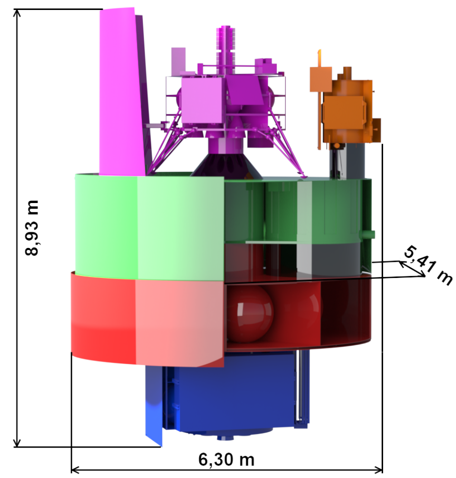

Fig. 1: Launch configuration. From the top: Hopper in pink, Science Orbiter in Orange, Orbital Module in green (solid sub-stage) and red (liquid sub-stage), Transfer Module in blue.

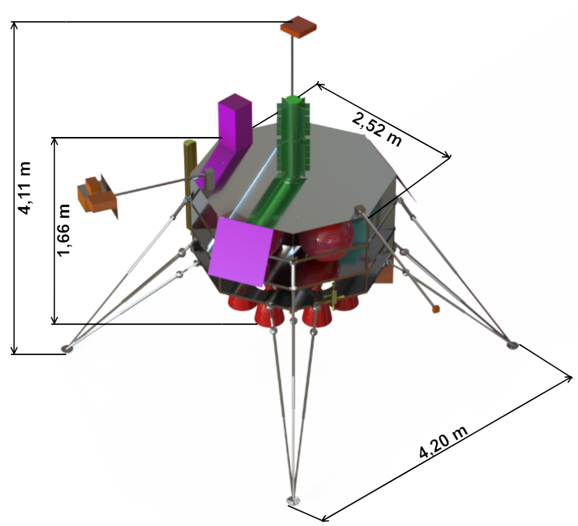

Fig. 2: Hopper rendering with dimensions.

Figure 2 shows the rendering and the dimenstions of the Hopper in the deployed configuration. The material used for the main body and the legs of the Hopper is Aluminum 7075 and a sandwich panel, made of AlBe Met and an Aluminum 5056 honeycomb, to optimize the mass. However, to be compliant with TCS requirements, the feet are made in a Titanium alloy (Ti-6Al-5Zr-0.5Mo).

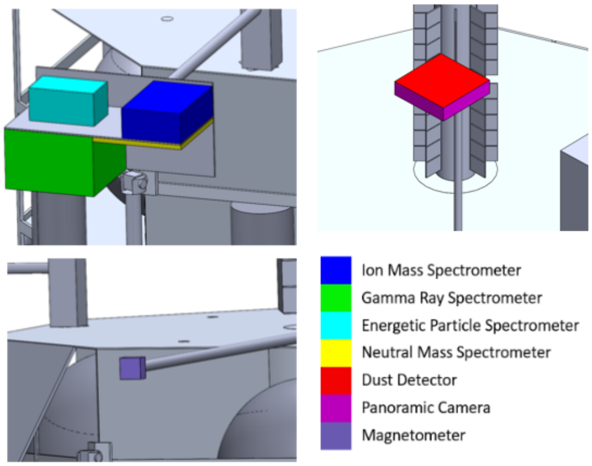

Fig. 3: Hopper robotic arms configuration.

The Hopper's design aims to achieve a compromise between the requirement for accurate pointing and positioning of its several parts, with a particular emphasis on the payloads and the Radioisotope Thermoelectric Generator (RTG). It is necessary to keep the RTG away from electronic components since its radiation can cause malfunctions. Key components of the Hopper consist of:

- Payloads: The Hopper has three robotic arms in which some of the payload are placed, as shown in Figure 3. The Ion Mass Spectrometer (IMS) and Energetic Particle Spectrometer (EPS) are positioned on rotational arms to face deep space. Gamma Ray Spectrometer (GRS) and Neutral Mass Spectrometer (NMS) are placed on rotational arms to ensure they point towards the surface. The Dust Detector (DD) and panoramic camera are on deployable arms, positioned to avoid RTG interference. The accelerometer is mounted on a foot for accurate measurements. The regolith imager is placed on the drill arm, X-Ray Diffractrometer/Fluorescence (XRD/XRF) inside the main body.

- Cameras: Descent cameras are on the bottom face to capture the surface during landing.

- RTG: Located on top of the Hopper to manage launch loads and keep it away from electronics and engine heat.

- Engines and Tanks: The Hopper has 9 engines and 5 tanks, with careful placement to balance the center of mass.

- Antennas: Phased array and bi-cone antennas are positioned for optimal Earth communication.

- Drill: Placed on an external face of the Hopper

- Radiators: Deployable and detachable radiators are installed to manage thermal requirements, positioned laterally on opposite faces.

- Sun Shield: A sun shield is mounted on a different module in front of the Hopper to protect it from direct solar radiation, ensuring thermal control during the mission.

- Electronic components: Electronic components are placed inside the body of the Hopper and distributed in order to minimize the displacement of the center of mass from the geometrical center.

IV. Reaching The Sampling Locations

In order to ensure a propellant efficient and reliable landing, a tradeoff between the possible propulsion solutions has been performed. To slow down the module and prepare for the landing maneuver large solid rocket boosters (TP-H-3340) have been selected, allowing for high thrust, reliability and relatively high specific impulse. The high thrust level allows to reduce the maneuvering time and thus the gravity losses during the maneuver. On the other hand, for the landing and hopping phases liquid propellant engines (HYD-MON3) allow for a soft and precise landing, as well as reignitability and throttlability for the hopping phase.
For these phases it is worth using the same engines that were used for the landing phase: since the fuel mass for landing is not high and the characteristics required are very similar there is no need to perform another staging and leave inert mass in the first landing site. Furthermore, since the mission requires two hops the staging technique is not convenient: three different sets of engines and legs for landing would be required, increasing consistently the inert mass.
It is important to point out that the space needed to place the 9 engines leads to a Hopper diameter of around 1.5 meters. Having 9 engines allows the Hopper to have an engine failure and still be capable of achieving a T/W around one in the landing phase, so that the landing is still correctly performed. In this case, however, the second jump would be unfeasible to perform due to the higher amount of propellant used in the previous phases. In further analyses an engine modification to enlarge the thrust level can be considered to achieve single failure tolerance, but

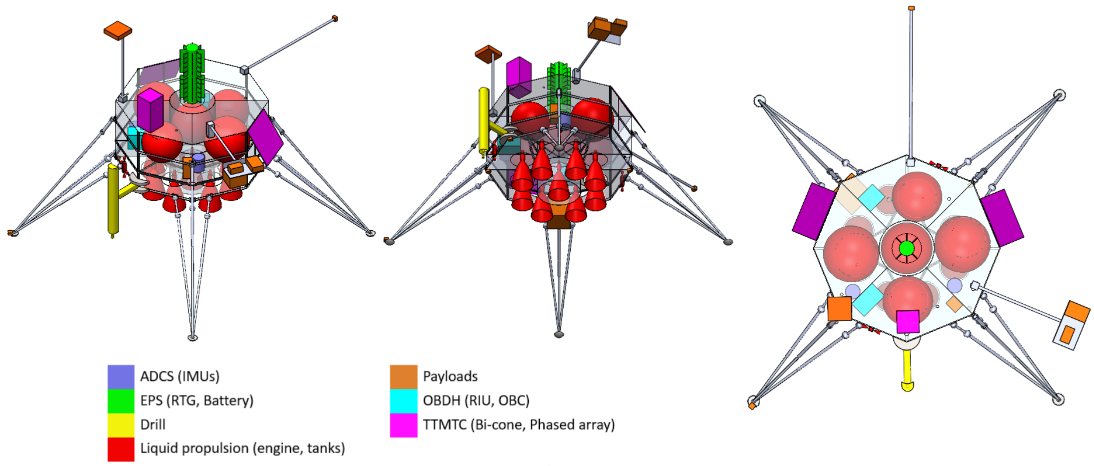

Fig. 4: Hopper configuration.

this solution would lead to a higher total mass of the system.

IV.i Simulator

In order to precisely estimate the propellant mass for the descent, landing and hopping maneuvers, a simulator is necessary. To avoid too long simulations, the problem has been divided in 3 parts: one for each jump and another one for the descent and landing maneuver. For each one of these parts an independent simulator has been built. The simulator integrates the equations of motion, retrieving the final conditions. The approach used is the single shooting, discretizing the trajectory in small segments in which the gimbal angle and thrust level are constant, allowing to obtain the time discrete optimal control law in terms of throttling ad gimbal angles. Once the simulator has been validated, it has been fed into a '`particleswarm`'+'`fmincon`' global optimization algorithm to retrieve the optimal trajectory. The goal of the optimization is to reduce as much as possible the propellant needed to match the final conditions desired. The equations of motion used are the ones reported in Equation (1), under the assumptions of dot mass, 2D motion, no aerodynamic effects and round planet.

$$\begin{cases} \dot{S} = \frac{R_m}{r} v \cos\gamma \\ \dot{v} = \frac{T}{m}\cos\delta - g\sin\gamma \\ \dot{\gamma} = \frac{1}{v}\left(\frac{T}{m}\sin\delta - g\cos\gamma + \frac{v^2}{r}\cos\gamma\right) \\ \dot{r} = v\sin\gamma \\ \dot{m} = -\frac{|T|}{I_{sp} g_0} \end{cases} \quad [1]$$

Where S is the downrange, v is the magnitude of the velocity, γ is the direction of the velocity with respect to the local horizon, δ is the gimbal angle, r is the distance between the center of Mercury and the spacecraft and m is the mass of the system. Moreover the thrust can be either positive or negative depending on the phase, if it's meant to slow down the spacecraft it will be negative, if it's used to increase the velocity it will be positive. In further developments a 6 DoF model can be implemented to simulate a more realistic behavior accounting also for the complete attitude of the module, but up to now this 2 DoF plus gimbal model is considered a good approximation. It is important to underline that these assumptions have been necessary in order to reduce the computational effort, in fact to simulate the 6 DoF behavior of the vehicle a more powerful computing unit would have been necessary. However, this is an acceptable approximation for this phase of the design.

IV.ii Descent and landing

Since the descent and landing maneuvers are very dependant one from the other in the algorithm both of them have been optimized at the same time in order to retrieve the overall mass optimal trajectory. The dry mass for the Orbital Module solid has been retrieved from the mass budget, resulting to be 1125 kg and the Hopper inert mass retrieved was 1710 kg, being the actual inert mass plus the propellant mass needed for the hopping phase.

The target values of $\gamma = -90$ deg (vertical landing) and landing velocity of 1 m/s are achieved within acceptable ranges. The resulting trajectory is reported in red and yellow in Figure 5, while in blue is reported the propagation of the orbit obtained with the pericenter lowering burn, performed to prepare the Hopper for the landing phase. In Figure 6 is reported the thrust profile retrieved from the optimization for the landing phase.

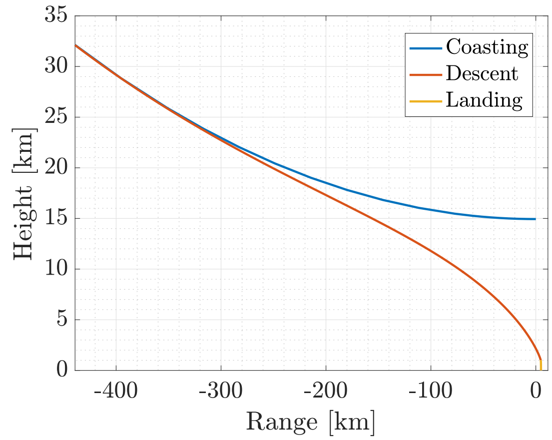

Fig. 5: Descent and landing trajectory

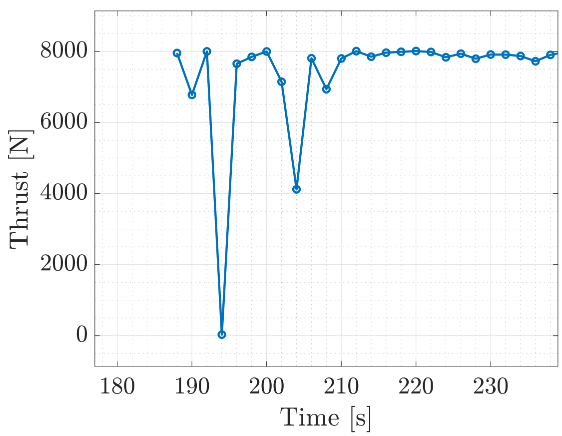

Fig. 6: Landing thrust profile

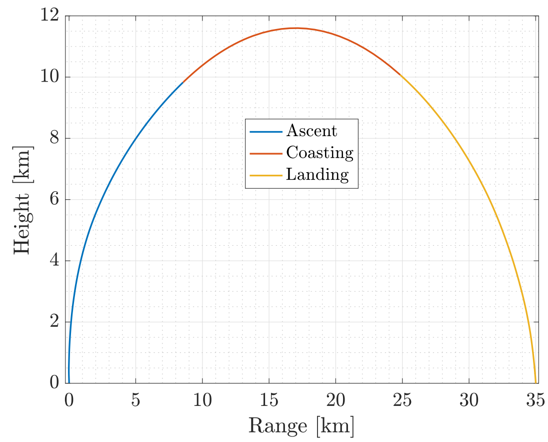

Fig. 7: First jump trajectory

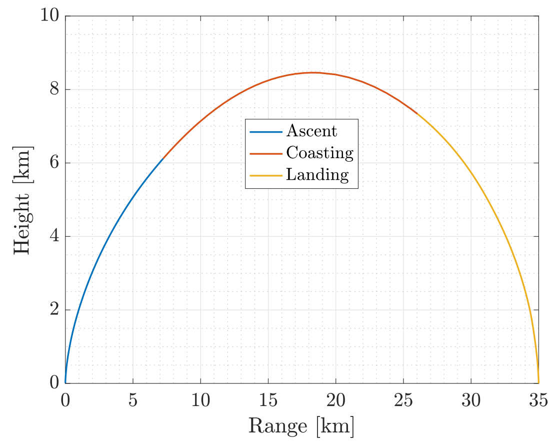

Fig. 8: Second jump trajectory

IV.iii Hopping

In the simulator the hopping maneuver has been divided in three main phases: an ascent, a coasting and a landing phase. Through the optimization process it has been possible to retrieve the mass optimal solution to perform the jumps on Mercury surface. The inert mass of the second jump was set to 790 kg (Figure 7), while the inert mass of the first jump was 1100 kg: the inert mass of the Hopper plus the propellant mass needed for the second jump (Figure 8). Also in this case the target values of $\gamma = -90$ deg and landing velocity of 1 m/s are achieved within acceptable ranges as well as the target distance of 35 km.

IV.iv Montecarlo analysis

Once all the optimal trajectories have been retrieved it was necessary to assess the landing precision according to the estimated uncertainties through a Montecarlo analysis. In order to have a significant output a 3D trajectory propagation model was implemented and validated through the results of the 2D simulator.

The results obtained show that also in the worst case the Hopper is expected to land within the significant location from a science point of view. Moreover, it is important to underline that the landing precision will increase once the control system will be implemented. The Montecarlo has not been performed for the hopping phases: the system will be capable to detect the real landing position and the new optimal trajectory aiming to the second landing spot can be uploaded from ground. This will lead to a very precise landing, also thanks to the onboard control system that will be developed.

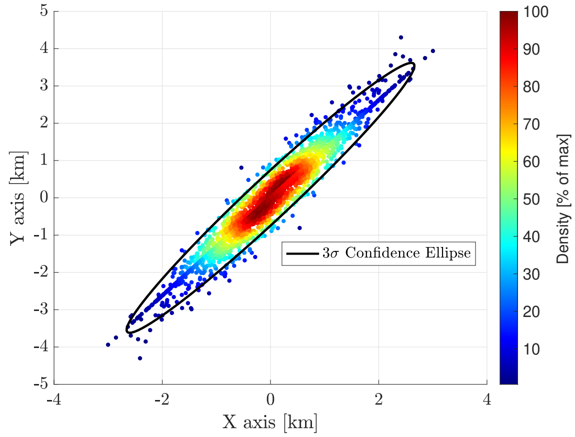

Fig. 9: Montecarlo results

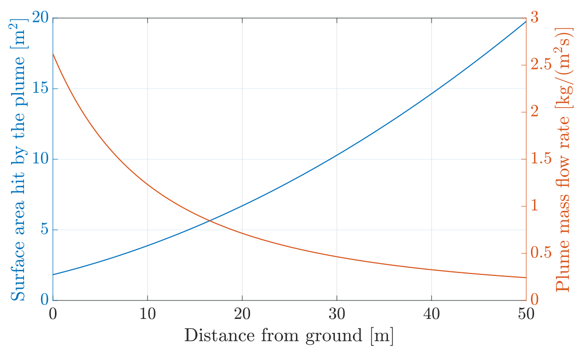

Fig. 10: Area hit by the plume and mass flow rate per square meter vs distance from ground

IV.v Engine plume pollution analysis

Once landed, the Hopper possesses an equivalent mobility to that of a lander. Hence, it is crucial to minimize the impact of the landing on the surrounding environment, which will subsequently serve as the sampling area. To this end, preliminary analysis of surface pollution induced by the engines during landing was conducted in a two-step process.

Mechanical analysis The first step involved assessing the mechanical impact of the plume on the surface. It is important to asses whether the plume is expected to cover entire area reachable by the Hopper sampling arms, or if only a part of it would be affected. In this last case there would be the possibility to sample a little further away from the landing site by increasing the sampling mechanism boom length. This analysis has been conducted focusing on examining the surface directly impacted by the plume particle stream via a simple flux-tube mass conservation of the exhaust plume for different altitudes during landing.

From the results shown in Figure 10 was observed that a stream of nearly 2 kg/s affects an area of 2.7 m^2 when the Hopper is positioned at a 5 m height from the ground while roughly 0.7 kg/s hit an area of 6.7 m^2 at 20 m height. Consequently, sampling is likely to occur in a contaminated area, and the chemical composition of the soil will be influenced by the engine exhaust plume. This impact needs to be considered when the scientific data are retrieved from the first layers of soil.

Chemical analysis The second phase of the analysis is concentrated on identifying the pollutant elements introduced by the exhaust plume through a chemical analysis of the engine's combustion products. Employing the NASA CEA program and considering a finite dimension thrust chamber, the hypergolic couple burns, yielding the following combustion products: 40% N_2, 18% H_2, 39% H_2O, 2% others (including H, NO, N_2, O, OH, O_2). Consequently, data collected from the first layers of soil must consider the concentrations of these elements as background noise. These concentrations need to be subtracted from the results of the scientific analysis to obtain accurate and meaningful insights.

In order to create a meaningful database of the polluting elements induced by the landing and their concentrations, further developments will analyze the chemical species which will form up when the hot exhaust plume enters in contact with Mercury surface elements. Furthermore, a more accurate combustion mechanism analysis would be needed in order to determine the non-equilibrium reaction products and the actual concentration of particles that will be present in the different locations will be assessed performing an analysis on the impact and bouncing back of the exhaust stream flow.

IV.vi Control strategy

During the descent, the control authority is guaranteed through the Orbital Module solid, which employs Star Trackers and Inertial Measurement Units (IMUs) for attitude determination and propagation [2]. Eight 22 N thrusters in 45° configuration are chosen for attitude control, to guarantee controllability of the vehicle even in case of a possible thrust misalignment of the descent burn. The misalignment is minimized by assigning the control authority of the gimbal of the main thruster to the ADCS of the Orbital Module for coupled attitude-gimbal control.

During the landing and hopping operations, Anubis

ADCS was strictly coupled with the GNC subsystem to maximize coordination between attitude and trajectory control. To control the attitude eight 4 N thrusters in 45° configuration were used. Attitude control is coupled with the main engines thrust control and vectoring to fully control Anubis during the large maneuvers of lift-off and landing. The 45° configuration of the thrusters allows to reduce the number of the necessary thrusters to eight, simplifying the configuration. The duration of the hopping does not accumulate significant drift on the IMUs, which are used to propagate attitude and trajectory without the need of additional Star Trackers. The IMUs bias is continuously estimated and corrected by the navigation filter. Navigation cameras and an altimeter are employed to safely control the landings with image processing algorithms [3].

IV.vii Suspensions

Due to the multiple jumps of the Hopper, a reusable suspension system has been considered. The design options considered included hydraulics, pneumatics, active magnetic, and passive electromagnetic systems. Hydraulic systems were disregarded in [...] [...] the initial concept selection due to their incompatibility with space conditions. Pneumatics, compressible and non-Newtonian fluids, were also discarded due to the complexities associated with pressurization and sealing in space environments. Active magnetic systems were ruled out due to their power consumption, leading to the selection of a passive electromagnetic system with a permanent magnet. To establish the parameters of the damping system, a thorough understanding of the forces acting on the legs was necessary, so a mathematical model was devised to calculate the dynamic forces exerted on the legs upon touchdown. The best method to model the landing is by using energy and work to determine the equations of motion, so a Lagrangian approach. The complete procedure can be seen in [4], here will be reported only the final equation of motion, shown in Equation (2). First of all the mass of the Hopper was considered punctual in its center of mass and each leg was divided into a primary strut, consisting of a single beam with a spring-damper system, and a secondary strut, formed by 3 beams with a spring-damper system each.

$$\begin{cases} m\ddot{z} + mg - k_p\left(\dfrac{l_{p0}}{l_p} - 1\right)(z+b) - 3k_s\left(\dfrac{l_{s0}}{l_s} - 1\right)(z+d) = -\dot{z}\left[c_p\dfrac{(z+b)^2}{x_1^2+(z+b)^2+y_1^2} + 3c_s\dfrac{(z-d)^2}{x_1^2+(z-d)^2+y_2^2}\right] \\ l_p = \sqrt{(x+a)^2+y_p^2+(z+b)^2} \\ l_s = \sqrt{(x+c)^2+y_s^2+(z+d)^2} \end{cases} \tag{2}$$

Here m is the total mass of Anubis, g is the gravity constant of Mercury,z is the vertical position of the center of mass, k_p and k_s are respectively the spring constants of the primary and secondary struts, with a value of $k_p = k_s = 3000\ N/m$ in the same way, c_p and c_s are the respective damping constants of the primary and secondary struts, also this time taken the same with $c_p = c_s = 3500\ Ns/m$. The parameters a, b, c, and d are distances from the center of mass with regard to the reference frame presented in Figure 11.

A preliminary worst case was analyzed, it consisted of simulating the maximum force that a leg would have to bear, considering maximum vertical and horizontal velocity into a 10° slope. To simplify the problem, some assumptions were made: for the first 0.25 seconds one leg will have to support the entire weight of the Hopper alone; after this transient period, the weight will redistribute across all four

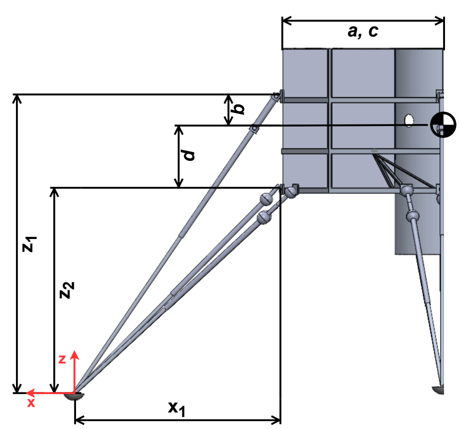

Fig. 11: Reference frame of the suspension's mathematical model.

legs again, also the landing velocity was doubled with respect to the nominal one to be more conservative. The results showed a maximum vertical acceleration of 30 m/s^2 that was margined by 60% to account for the simplicity of the model. Thus, in the worst case the main body and the legs need to survive to a margined acceleration of 50 m/s^2 during the landings. It is important to perform a structural analysis. From the static structural analysis, a safety factor of 1.39 and a maximum displacement of 7.3 mm were obtained. These results are compliant with the suspension requirements.

V. Surviving the Extremes

V.i Extreme temperatures

The Hopper will experience significant variations in external heat fluxes throughout different phases of the mission, playing a pivotal role in shaping the overall mission design. As a result, this analysis focuses on examining these external fluxes, as they will exert a substantial influence on the choices made in the design of the TCS later explained. Ultimately, the analysis will concentrate solely on the phase in which the Hopper operates on the surface.

Descent and Landing: During descent, aerodynamic heating will not be encountered, as Mercury has no atmosphere to cause friction. However, temperatures can still rise significantly due to the dissipation of the engines. As the S/C descends towards Mercury's surface, the propulsion systems may generate heat that needs to be effectively managed. Heat dissipation mechanisms, such as radiators or other thermal control systems, must be in place to prevent the temperature from reaching levels that could compromise the integrity of the Hopper and its instruments.

Surface Operations: Mercury's surface temperatures exhibit dramatic variations, with daytime temperatures soaring to around $450°C$, while nighttime temperatures plunge to approximately $-160°C$. Notably, operations on Mercury's surface are exclusively planned for nighttime, when the consideration of albedo influence is not required due to the absence of direct solar radiation. During nighttime operations, the Hopper on Mercury's surface will experience reduced infrared flux emitted by the planet. In fact, as the environment cools during the night, the emitted IR flux diminishes. While external factors like solar and planetary IR flux decrease, internal dissipations within the Hopper become particularly noteworthy. In this context, effective thermal control systems remain paramount. A key player in managing internal dissipation is the RTG, which provides a crucial 3040 W of power. The heat generated by the RTG can be smartly exploited to regulate internal temperatures, preventing the Hopper from becoming too cold during nighttime operations. Strategic insulation and heating systems, in conjunction with the RTG, become critical elements to ensure the Hopper's functionality and safeguard instruments from the challenges posed by the extreme thermal environment on Mercury, specifically tailored for nocturnal operational conditions.

Operational Duration: During the 3-month surface operation period, the Hopper and its instruments will undergo thermal cycles, presenting a challenge that requires robust thermal management systems for optimal performance. This involves a combination of passive elements like insulation to buffer temperature fluctuations and active systems such as heaters and cooling mechanisms. Maintaining operational temperatures within the specified range is crucial, not only for immediate functionality but also for the long-term survivability and reliability of the Hopper and its instruments.

A substantial heat contribution came from the dissipation of internal components. In order to size the TCS for worst-case hot and cold scenarios, the onboard power dissipation is set equal to the power budget in different phases, as shown in Table 1.

Segment	**Power [W]**
Hopper	3123.84 / 3040

Table 1: Hopper power budget for hot and cold cases.

The dissipation scenarios outlined in this study were deliberately selected for thermal analysis, emphasizing their prolonged durations in contrast to brief events in specific modes. This careful selection facilitates the exploration of potential steady-state temperature ranges. For instance, the power consumption of the Hopper in idle mode was included, with the efficiency of 65% applied. Furthermore, the analysis considered the waste heat from the RTG. For the Hopper, the power consumption in the hot case was assumed to be in science mode, as it represents the most demanding mode to be sustained over an extended duration. In terms of cold cases, the Hopper consistently dissipates 3040 W, representing the continuous heat generated by the RTG.

Acknowledging the inherent limitations of the mononodal thermal model in fully capturing the thermal intricacies of the Hopper, a more nuanced analysis was pursued through a multinodal model, as illustrated in Figure 12. This thorough examination sought to unravel the combined effects of the implemented control strategies. The model comprises 4 nodes: the main body of the Hopper, the battery (emerging as the most thermally influential component due to its restricted temperature range), the OBC (recognized as the most heat-dissipating component), and the RTG. In the case of the main bus, the second most limited temperature range has been employed, mirroring that of the tanks (ranging from $0°C$ to $45°C$, accounting for a $15°C$ margin). Given that these analyses focus on the Hopper situated on the Mercury surface, the sunshade node is excluded, considering its deployable nature. As depicted in Figure 12, the model also incorporates conduction with the surface of Mercury. All nodes are interconnected through conduction, supported by a titanium structural system that prevents excessive fluxes between each node in the hot case. View factors with Mercury are computed with the Hopper on the surface, treating the planet as a homogeneous sphere. It's crucial to highlight that, in the hot case, the dissipation is distributed as follows: 67.04 W in the main body of the Hopper, 1.6788 W in the OBC, constituting 10% of the 35% of the required power (considering the OBC is not at full power), and 3040 W for the RTG. Conversely, in the cold case, only the dissipation of the RTG (3040 W) is considered. This analysis aims to assess the Hopper's capability to endure dusk conditions with $q_{Sun} = 555W$, considering the surface temperature at 313 K, and accounting for Mercury's slow rotation. Following that, the considerations involve q_{IR} at 506 W, q_{albedo} at 40.97 W, and $q_{internal}$ without the sunshield for a minimum of 24 hours, as stipulated by the MA team.

The heat reaching the Hopper is moderated by the presence of Multi-Layer Insulation (MLI). Kapton MLI with values of $\alpha = 0.12$ and $\varepsilon = 0.03$ is employed [5]. In the hot case, particular attention is directed toward the link between the Radioisotope Thermoelectric Generator and the Hopper, employing titanium to minimize heat fluxes reaching the Hopper—critical given its stringent temperature requirements. Additionally, the connection between the Hopper's legs and the surface of Mercury utilizes copper (leveraging thermal straps) to enhance heat dissipation on the surface more effectively. Conversely, in the cold case, strategic use of the dissipation from the RTG is employed to sustain the Hopper's warmth without relying on heaters. This is accomplished by utilizing copper thermal straps to enhance thermal conduction between the RTG and the Hopper. Moreover, titanium [6] is applied at the bottom of the Hopper's legs to prevent heat flux loss to the surface of Mercury, assumed to have a mean temperature of $-163°C$. A comprehensive presentation of all results is available in Figure 13.

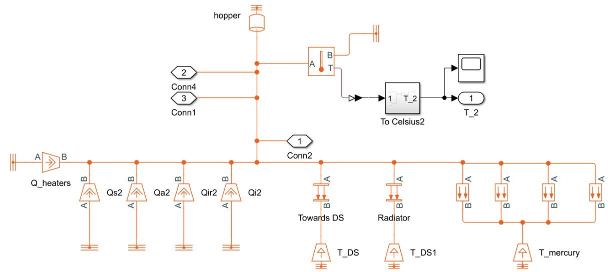

Fig. 12: Example of the thermal node of the Hopper bus.

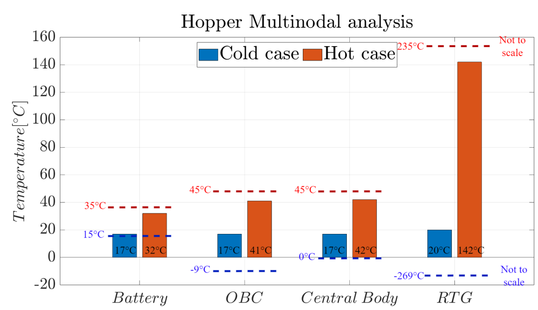

Fig. 13: Results for both the hot and cold cases.

In the hot case, the absence of radiators is deliberate. The radiators, which have been determined to be needed to cool down the hopper during previous phases, are anticipated to be deployable and detachable to assist the configuration team during the landing phase. Consequently, no radiators are situated on the surface in both the presented hot and cold cases. Temperature limits in both scenarios are skillfully maintained through strategic utilization of the RTG and the Mercury surface from a thermal perspective. In the cold case, no heater power is required thanks to the judicious use of the RTG. Conversely, in the hot case, MLI and thermal dissipation through the Mercury surface contribute to diminishing the heat flux, allowing the Hopper to endure for 24 hours. If the analyses are extended beyond this timeframe, the temperature limits would no longer be adhered to. In Figure 14, Figure 15 and Figure 16, the temporal evolution of temperature is vividly depicted, skillfully capturing the dynamic fluctuations over time. It is noteworthy that, as previously mentioned, the multinodal analysis demonstrates that acceptable temperatures can be attained without radiators and heaters, solely by leveraging the RTG dissipations and the thermal dissipations through the Mercury surface.

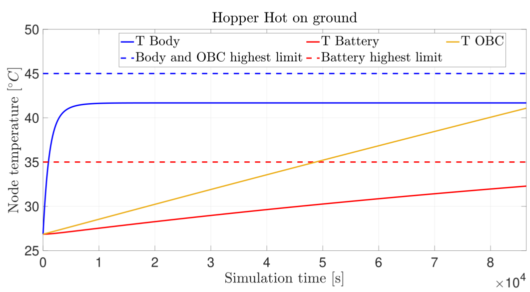

Fig. 14: Hopper on-ground hot case.

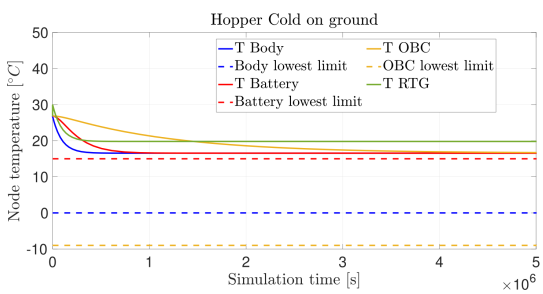

Fig. 15: Hopper on-ground cold case.

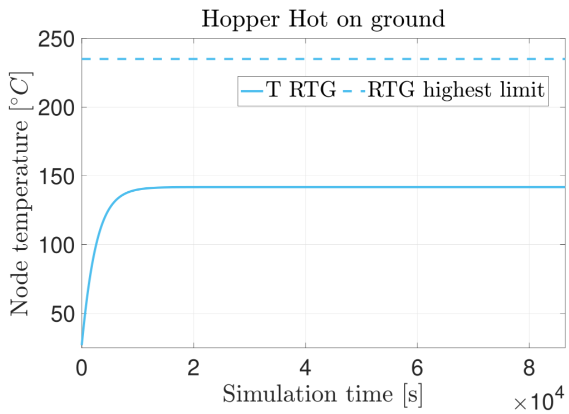

Fig. 16: RTG on-ground hot case.

Moreover, it is crucial to underscore that in this multinodal analysis, thermal nodes are not generated for the payloads, mirroring the absence of the most stringent temperature requirements. However, specific components within the Hopper, such as the Gamma-ray spectrometer and X-ray diffractometer, operate at significantly lower temperatures compared to the rest of the Hopper. Consequently, traditional thermal control methods involving heaters and radiators are insufficient, necessitating an oversized approach. Therefore, the proposed thermal solution involves the implementation of dedicated cryocoolers exclusively for these payloads. According to Figure 17 and considering their respective operational temperatures, this approach is estimated to result in a power consumption of approximately 25 W per cryocooler, a value that will be prudently margined and accounted for. This graph is referring to the Lockheed Martin "Micro" pulse-tube crycooler [7].

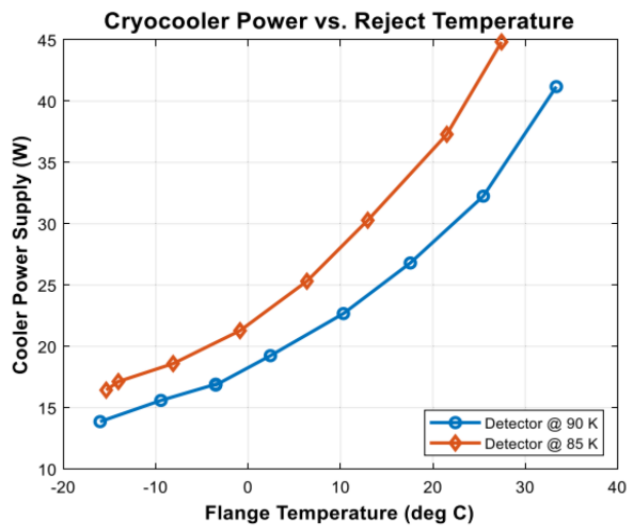

Fig. 17: Power consumption of the cryocooler correlates with temperature.

V.ii Power generation

Due to the intense solar flux during daytime, the ground segment is constrained to operate mainly during night in order to be able to survive. For this reason any photovoltaic solution is excluded, thus the two most promising alternatives as primary power source are nuclear energy and primary batteries. In particular, the 16 GPHS NextGen RTG was preferred as it showcases a long design life ($17 years$) and a considerable energy output to accommodate all the mission needs [8]. On the other hand, primary batteries are able to provide power for a maximum duration in the order of tens of hours which is far below the minimum requirement of surviving at least 90 days. Plus, it is worth mentioning that the system's landed mass would have been increased by their lower specific energy (up to $400\,Wh/kg$), endangering the proposal's feasibility. Other strengths of the NextGen RTG include a higher efficiency with respect to the ones employed in current space missions (16.5% vs 6%) and a static conversion principle based on the Seebeck effect which boasts a reliability equal to the state-of-the-art RTGs.

To verify the feasibility of the choice, the RTG power output must be compared with the Hopper's power budget per each phase and mode reported in Table 2.

Phase/Mode	P_{req} **[W]**
Nominal	302.4
Safe-hold	130.7
Appendages deployment	213.1
Landing	779.6
Hopping cruise mode	321.7
Maintenance & calibration	381.6
Lift-off	767.9
Orbiter communication	277.9
Sampling acquisition	555.4
End-of-life	136.6

Table 2: Hopper power budget.

For sizing purposes, the annual degradation (d_{year}) due to the radioactive material's decay during interplanetary cruise is estimated to be about 1.6%, knowing that the power at BOL (P_{BOL}) and EOL (P_{EOL}) is 456 W and 347 W, respectively. Plus, the time needed to reach Mercury (T_{cruise}) was considered 8.6 y as dictated by the trajectory analysis. "Nominal" mode is used for sizing as it is the most used throughout the whole mission lifetime, while P_f is the power output after the interplanetary cruise.

$\mathbf{P_{req}}$	$\mathbf{P_{BOL}}$	$\mathbf{T_{cruise}}$	$\mathbf{P_f}$	**Margin**
$302.4\,W$	$456\,W$	$8.6\,y$	$397.1\,W$	$94.7\,W$

Table 3: Hopper RTG sizing.

Table 3 shows a substantial power margin for the "Nominal" mode, showing that the chosen RTG is a suitable choice for the case. The same also applies in all the other cases with the only exception of "Sampling acquisition", "Landing", and "Lift-Off" in which the RTG output is not enough to sustain operations, thus demonstrating the need of a secondary power source.

The "Sampling Acquisition" mode was considered for sizing the battery despite its lower power consumption ($555.4\,W$) with respect to the other two because of its long duration (T_{op}), which leads to an overall higher energy required. The power provided by the RTG is subtracted from the one required by the mode to obtain P_{req}, which is used in the sizing process. By taking into account the typical values for Depth-Of-Discharge (DOD) and efficiency (η) of Li-Ion batteries, the required capacity (C_{req}) can be obtained.

$\mathbf{P_{req}}$	$\mathbf{T_{op}}$	**DOD**	η	$\mathbf{C_{req}}$
$158.3\,W$	$514\,s$	80%	95%	$1.1\,Ah$

Table 4: Hopper secondary battery sizing.

For a refined topology sizing, the battery operating voltage (V_{sys}) has been set equal to the one of the RTG (28 V) and the packaging factor μ is considered 80%. For the single cell's voltage and capacity (V_{cell} and C_{cell}), typical values have been chosen [9]. Plus, the final capacity C_{real} includes also an additional string for redundancy to take into account the hypothesis of one battery cell failure.

$\mathbf{V_{cell}}$	$\mathbf{C_{cell}}$	$\mathbf{V_{sys}}$	**Topology**	$\mathbf{C_{real}}$
$3.6\,V$	$4.5\,Ah$	$28\,V$	8s2p	$7.2\,Ah$

Table 5: Hopper's battery topology refinement.

V.iii Footpads

To ensure proper stability and a safe departure with each jump, it is essential to prevent Anubis from sinking upon landing. This requires a preliminary study of the footpads: a larger surface area decreases the depth of penetration into the ground compared to a smaller area since its shape influences the friction force on it. At the same time, it increases the thermal exchange with the ground. To simplify the initial design phase, a generic spherical shape was chosen for the footpad, defined by its diameter (D_f), height (L_f), and thickness (t_f). A basic technical illustration of the footpad is shown in Figure 18.

The surface of Mercury was assumed to resemble lunar regolith, guiding the determination of the minimum contact area required between the footpad and the soil to ensure stability and safety. The final parameters for the footpad are listed in Table 6. It is worth noting that the thickness and material of the footpad were constrained by the TCS (Thermal Control Subsystem) requirements.

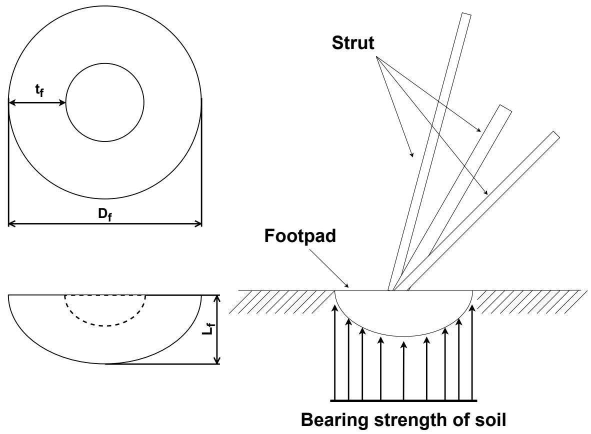

Fig. 18: Footpad geometry.

Parameter	Value
$\mathbf{D_f}$ [mm]	166
$\mathbf{t_f}$ [mm]	45
$\mathbf{L_f}$ [mm]	66
Mass [kg]	3
Contact Area [cm^2]	311
Material	TiAlZrMo

Table 6: Footpad main parameters.

VI. Deep Dive: Analysis

VI.i Surface sampling and collection

A drill was chosen to ensure proper sampling. The selection of the drill type was influenced by multiple considerations, such as the variability of the three sampling locations, the low-gravity environment on Mercury, the risk of sample contamination, and the stationary nature of the Hopper after touchdown. To address these factors, an USDC (Ultrasonic/Sonic Driller/Corer) was evaluated as a viable option. The USDC consists of three primary components: the actuator, the free mass, and the bit. The actuator serves as an ultrasonic vibration mechanism, delivering energy to the free mass, which then impacts the bit, producing a stress impulse. This impulse enables rock fracturing at the rock/bit interface when the ultimate strain of the rock is exceeded. The effectiveness of the USDC has been demonstrated through the successful drilling of various materials [10] such as ice, granite, diorite, basalt, and limestone. Its adaptability across diverse terrains is due to the integration of an interchangeable bit mechanism and a bit tool caddy within the drilling apparatus. This system can also function as an emergency ejection mechanism if a bit becomes lodged in the substrate. For the MIRAGE mission, rather than exclusively utilizing a percussive excavation method, the system was enhanced by integrating a rotary penetration approach. This combination allows the drill to handle both harder terrains, where percussive action is more effective, and softer grounds. The two methods function independently, ensuring redundancy if one fails. Moreover, they can be used concurrently to expedite excavation operations. Furthermore, the drill was designed to autonomously collect the produced samples, drawing inspiration from the *Dragonfly* mission, which uses a blower [11]. Once the drill's structure was established, its impact on the overall Hopper system needed careful consideration. The primary concern centers around the imbalance generated by the force exerted by the drill on the surface, which can reach over 1000 N, depending on the terrain characteristics. This force can create a moment that, under the low gravity condition in Mercury, may lead to instability or even tipping of Anubis. To address this potential issue, ground-anchoring harpoons were proposed to stabilize the system during drilling operations. An additional factor that may affect other subsystems is the driving voltage of the actuator. For optimal performance, a sinusoidal DC voltage must be generated using a dedicated modulation system.

VI.ii Analysis of surface/subsurface

Surface analysis on Mercury involves capturing detailed images and collecting samples. The regolith camera, positioned near the drill, captures detailed images of the texture and particle size of the surface material before and after each sampling operation. This enables a detailed examination of any changes in the regolith's physical characteristics, providing data to assess the quality and composition of the sample collected during drilling. Instruments like the EPS, NMS, IMS, and DD run continuously, sampling every ten seconds to monitor the fluctuating exosphere and magnetosphere. The magnetometer will take surface measurements of the vector magnetic field with the precision of 1 nT, which will help us gain insight into its interior structure, and improve our understanding of exospheric processes like surface precipitation. The panoramic camera is another payload that captures the characteristics of dust particles. It operates best in daylight due to its need for light, but it can also function at night with the assistance of sodium illumination from the surface, which has specific wavelength properties that improve the contrast and visibility of fine dust particles without saturating the camera's sensors. The Accelerometer measures vibrations and changes in gravity and can function as a seismometer. It can measure noise-free data in three dimensions and collect continuous data at speeds of up to 100 frames per second.

The sub-surface analysis uses the XRD/XRF instrument for mineralogical and geochemical studies, requiring other instruments to pause while functioning due to power constraints. When samples are collected by the drill into the sampling tray, they are first analyzed for an hour to gather initial data. After several days, the same samples undergo a more in-depth examination that lasts for four hours to gain further insights. Cross-contamination is prevented through the flushing of the supply lines using gas between sampling events to clear residual material. The GRS, after a 36-hour cool-down period upon landing, can detect the elemental composition of the sub-surface by analyzing gamma rays reflected from up to one meter beneath the surface.

Operations span three landing sites: 20 days at Landing Site I, 47 days at Site II, and 23 days at Site III, with direct communication established between the Hopper and Earth only during the operations at Sites I and III. Data collected at Site II is transmitted when the Hopper moves to Site III. This schedule and instrument usage provide crucial insights into a better understanding of the Mercury's geology and formation.

VII. Data Flow

The transfer to Earth of all the data collected by the payload is crucial for the mission's success, making a reliable communication subsystem essential. The TMTC architecture shall withstand Mercury's harsh environment and a long silence period in the middle of the mission due to the overlapping of a superior conjunction and the rotation of the planet. In addition, the presence of dust and loads during the multiple landings of the Hopper may interact with the deployment and pointing of the antennas, and the long distance from Earth (1.48 AU) strongly affects the power of the communication signals.

The overall scientific return of the mission includes a total of 11.5 GB of scientific data, mostly coming from the accelerometer, magnetometer and ion mass spectrometer which operate continuously and from the cameras acquiring daily images. The data shall be downlinked during the two visibility windows at the beginning and at the end of the mission and shall be stored on the OBC during the silence period.

In the epoch selected for the mission the DSN ground station facilities provide the best visibility performances with 43.7 days of available link with the Hopper. The visibility is mainly affected by the rotation of Mercury causing the set of the Earth in the Hopper's location for 46.3 days in the middle of the mission. The direct visibility window is divided in two long periods of 20.3 and 23.4 days at the beginning and at the end of the mission. Eventually, the second window can last more in case of a mission extension. Table 7 presents the results of the visibility analysis: the total link duration and the number of passages on each DSN ground station. Passages on Goldstone and Madrid have a median duration of 11 hours, while passages on Canberra last around 6 hours. The Hopper mostly rely on the first two ground stations providing longer coverage and lower atmospheric losses (in particular Goldstone). However, the presence of Canberra as third ground station guarantees a continuous communication in the two long direct Earth visibility windows.

During the silence period the apocentre of the Science Orbiter lies on the Hopper's location guaranteeing 9.3 days of communication with the Hopper, split in 48 passages, and 7.0 days of relay communication with the Earth.

Communication From To	**Duration** [days]	**Passages** G	M	C
First Direct Earth Window 2043-05-23 - 2043-06-12				
Hopper2DSN	20.35	19	20	20
Hopper2Relay	0.11		2	
Long Silence Window 2043-06-12 - 2043-07-28				
Hopper2DSN	0	0	0	0
Hopper2Relay	9.34		48	
Relay2DSN	40.68	40	41	51
Second Direct Earth Window 2043-07-28 - 2043-08-21				
Hopper2DSN	23.36	24	24	23
Hopper2Relay	1.31		5	
Total				
Hopper2DSN	43.71	43	44	43
Hopper2Relay	10.77		55	

Table 7: Visibilities.

Based on the data budget and visibility analysis, the science downlink to the DSN requires a maximum data rate of 377.4 MB/day during the mission's second visibility window. In a contingency scenario where data must be transferred to the orbiter, the maximum required data rate increases to

2254 MB/day.
The selected architecture for the transmission of data includes two Ka-band high gain rectangular phased array antennas for science downlink, and an X-band bi-conical antenna for safe mode and for the transfer of data to the Science Orbiter in case of contingency. The configuration of the high gain antennas is studied to cover an Azimuth of 190° guaranteeing full Earth visibility also in case of hopping failure.
The HGA have a peak gain of 43 dBi and an area of $0.27\,m^2$. The use of a phased array eliminates moving parts, enhancing reliability and reducing the impact of thermal deformations on the antenna pointing. These antennas, proven by the MESSENGER mission to withstand Mercury's orbital environment, do not require robotic arms for pointing, which improves thermal control, reduces vibration transmission during hopping phases, and minimizes the risk of jamming from dust during landings.
The bi-conical antenna guarantee an omni-directional radiation pattern with a sufficient gain of 6 dBi to compensate the space losses during safe mode and the high data rates in case of Hopper contingency.
The data handling architecture is inspired by the BepiColombo mission. The On-Board Computer (OBC) has been selected to meet all requirements for computational power, RAM, and mass storage. The memory is sized to store all data produced when a direct Earth connection is unavailable, and the OBC is designed with internal redundancy for reliability.
Sensors and actuators are connected via the MIL-STD-1553 bus, while payloads interface through the SpaceWire bus. Due to the use of model predictive control, an Attitude Determination and Control Subsystem (ADCS) board is required, and a payload controller is included to ensure reliable payload operations.
To offload tasks from the OBC, a Remote Interface Unit (RIU) is utilized, and a SpaceWire router is necessary to manage the high number of payloads. The OBC connects to both the RIU and the router, serving as a backup in case of failure.
To facilitate a controlled detachment of cables between vehicles, zero-force connectors are employed.

VIII. Final Thoughts

Here some final considerations about the mission as a whole are presented. Science Orbiter, Orbital and Transfer Modules have not been previously analysed since they are out of the scope of this work. Nevertheless, they are considered in this section to present a complete mission-level budget of the whole architecture needed to bring the Hopper on the surface of Mercury.

Segment	Mass [ton]
Hopper	1.97
Science Orbiter	0.38
Orbital Module	
Liquid	9.77
Solid	9.88
Transfer Module	5.54
Internal adapters	0.18
LVA	2.14
Total	**29.8**

Table 8: Mass budget.

Table 8 shows the mass budget of each segment of the mission. It is clear that the most critical stage is the Orbital Module. Its large mass is due to the enormous amount of propellant required to inject into Mercury orbit and land almost 2 tonnes of Hopper on an atmosphere-free planet, which has a direct impact on the structural mass of the Orbital Module itself, leading to its huge total mass.

Segment	Power required [W]
Interplanetary cruise phase	
Transfer Module	12894.5
Orbital Module	1280.8
Science Orbiter	119.2
Hopper	83.5
On-orbit phase	
Orbital Module	278.3
Science Orbiter	4.8
Hopper	88.2
Science phase	
Science Orbiter	455.9
Hopper	302.4

Table 9: Nominal power budget per each phase.

Table 9 shows the power required by each module in nominal operations per each mission phase. During the interplanetary phase, the Transfer Module solar arrays powers both this module itself and the Orbital Module, while the RTG provides power to the Science Orbiter and Hopper. In the On-orbit phase the Transfer Module has been jettisoned and the RTG powers the overall spacecraft except for the heaters working in non-nominal conditions. This architectures clearly demonstrates that the RTG is a crucial piece of hardware in any mission phase.

VIII.i Costs

Segment	Cost [FY2024 M€]
Hopper	154
Science Orbiter	300
Orbital Module	94
Transfer Module	395
Launcher	1064
LOOS	2.14
DSN use	2.14
Total (unmargined)	**2.06 B€**
Margin	50%
Total (margined)	**3.09 B€**

Table 10: Mission cost.

The total cost of the mission has been estimated using state-of-the-art cost estimating relationships. The hardware cost was estimated using the USCM8 (Unmanned Spacecraft Cost Model) which is based on the total mass of the spacecraft. Since the spacecraft is very massive the cost raised accordingly. COCOMO81 has been used to estimate the software development cost, while the official DSN cost sheet has been applied to estimate the communication cost. The launcher cost has been estimated starting from the average cost per kg for heavy launchers. It is important to point out that launcher cost could possibly improve a lot if SpaceX Starship programme will be able to strongly reduce the space access cost as they claim. Table 10 resumes the cost of each segment of the mission. The margin has been used to take into account mission budget increase due to unknown-unknowns. It is needed since missions with similar technological innovations suffered from large budget increase.

VIII.ii Conclusion

To conclude, it is crucial to analyze the most critical aspect of the mission: the mass. Since this parameter has a direct impact on the total cost, it is important to analyze how to reduce it in order to retrieve a cheaper mission.

One of the most critical aspects of the mission is the mass of the descent stage (Hopper plus Orbital Module solid). The Δv that this stage has to provide in order to perform a soft landing on Mercury leads to an extremely high propellant mass due to the weight of the Hopper, which is almost 2 tonnes. Even if this is the only solution found which is capable of completely fulfill the mission requirements of sampling three different scientifically relevant environments (HRM, LRM and a young crater), a future iteration might consider de-scoping as a mass saving solution. This would for sure highly reduce the scientific return of the mission but would also lead to a less massive, and therefore potentially more economically-appealing, solution.

References

[1] Sean C Solomon, Larry R Nittler, and Brian J Anderson. *Mercury: The view after MESSENGER*. Vol. 21. Cambridge University Press, 2018.

[2] P. Espeillac L. Szerdahelyi S. Fugger et al. "The BepiColombo Attitude and Orbital Contol System". In: *14th International ESA Conference on Guidance, Navigation and Control* (2014).

[3] Vincenzo Pesce, Andrea Colagrossi, and Stefano Silvestrini. *Modern Spacecraft Guidance, Navigation and Control*. Elsevier, 2023.

[4] William S Gullotta et al. "Resettable landing gear for Mars hopper". In: *11th International Planetary Probe Workshop*. Vol. 1795. 2014, p. 8055.

[5] David G. Gilmore. *Spacecraft Thermal Control Handbook*. The Aerospace Corporation, 2002.

[6] *Ansys GRANTA EduPack software, ANSYS, Inc., Cambridge, UK, 2023*. URL: www.ansys.com/materials.

[7] Morgan Burks. "GeMini: A high-Resolution, Low-Resource, Gamma-Ray Spectrometer for Planetary Science Applications". In: (2020).

[8] National Aeronautics and Space Administration. *NASA Radioisotope Power Systems Program: Next-Generation RTG Study Summary 2017*. Tech. rep. NASA, 2017.

[9] *Saft batteries - Powering outer space for half a century*. URL: https://www.saft.com/market-sectors/aerospace-defense/space.

[10] Yoseph Bar-Cohen and Kris Zacny. *Drilling in extreme environments: penetration and sampling on earth and other planets*. John Wiley & Sons, 2009.

[11] Ralph D Lorenz et al. "Dragonfly: A rotorcraft lander concept for scientific exploration at Titan". In: *Johns Hopkins APL Technical Digest* 34.3 (2018), p. 14.